Magnetic Dipoles for Electromagnetic Multi-DOF Actuator Design

Kok-Meng Lee, Jungyoul Lim, Kun Bai

Abstract— **This paper presents a new method for solving the magnetic forces/torques of a multi-DOF spherical actuator that has more controlling inputs than its mechanical DOF. Unlike methods that based on the Lorentz force equation or the Maxwell stress tensor, which require computing the volume or surface integrals to derive the forces, the dipole force method presented here offers the magnetic force solution in closed form. We validate the dipole force model against published experimental data, and demonstrate its application in solving the inverse torque model of a multi-DOF spherical motor, which computes the required set of maximum current inputs for a given design specifications.**

Index Terms— actuators, force/torque model, spherical motor, wrist actuator

I. INTRODUCTION

Design and real-time control of a multi-DOF electromagnetic actuator requires solving the inverse torque model which determines a set of input currents to the electromagnets (EMs) for a specified magnetic forces/torques. Two common methods used in calculating the magnetic forces in a magnetic field are the Lorentz force equation and the Maxwell stress tensor. Both these methods require solving the magnetic field and computing the volume or surface integrals to derive the forces.

Existing techniques for analyzing electromagnetic fields and for designing and real-time control of a multi-DOF actuator utilizing permanent magnets (PMs) rely primarily on three approaches; namely, analytical solutions to Laplace equation, numerical methods and lumped-parameter analyses with some form of magnetic equivalent circuits [1]. The possibility of obtaining an analytical solution is often remote for devices with complex geometry. Perturbation theory and linear superposition can sometimes render a difficult problem solvable. However, even if an analytical solution is achievable, it often results in a series of space harmonics of non-elementary functions [2] [3] which have to be computed if a numeric solution to the problem is desired. Numerical methods (such as finite element method) offer a good prediction of the magnetic field for accurate computation of the magnetic torque [4] [5]. However, demanding computational time limits these numerical methods to off-line computation. In order to obtain closed-form solutions for design optimization and motion control of electromagnetic actuators, real-time computations have largely relied on lumped parameter approaches which generally yield only first-order accuracy. These approaches have difficulties in

achieving both accuracy and low computation time simultaneously. More recently, the interest to optimize the spherical motor design has led us to develop alternative techniques for analyzing electromagnetic fields of a multi-DOF actuator. This effort led to the distributed multi-pole (DMP) method [8] for computing the magnetic field of a permanent magnet (PM), upon which the effects of key design parameters on the torque performance of a SWM [7] were investigated. To reduce the volume integral for computing the Lorentz force to a surface integral, an equivalent single layer (ESL) model that approximates the magnetic field of a multi-layer (ML) coil was proposed in [8]. While the ESL model provides a relatively time-efficient approach to obtain the magnetic force on a thin coil, the modeling error however increases with coil thickness, particularly within the core. For compact spherical motors where thick EM coils are important for high torque-to-volume ratio design, a more accurate yet efficient solution for predicting the magnetic field and force of an EM is desired.

An alternative method is to compute the magnetic force in analogy to that on an electric charge by the Lorentz law. As shown in Fig. 1, we define a magnetic dipole (with charge strength m) as a pair of source and sink separated by a finite distance. The force **F** and torque **T** acting on the dipole can be written (in analogy to that on a stationary electric charge by the Lorentz law) as

$$\mathbf{F} = \mu_o m \left[\mathbf{H}_{R+} - \mathbf{H}_{R-} \right] \tag{1a}$$

$$\mathbf{T} = \mu_o m \left[\mathbf{R}_+ \times \mathbf{H}_{R+} - \mathbf{R}_- \times \mathbf{H}_{R-} \right] \tag{1b}$$

where μ_0 is free space permeability; H_{R+} and H_{R-} are the magnetic field intensities acting on the magnetic source and sink of the dipole respectively; and the subscripts R_+ and R_- are the corresponding distances from a field point. Equation (1) suggests a closed form for computing magnetic forces of an actuator if both PMs and EMs and their magnetic boundaries can be modeled as dipoles.
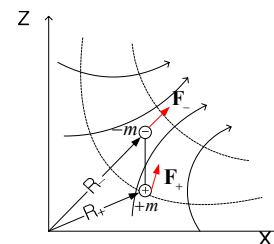

Fig. 1 Force on a dipole in the magnetic field

The remainder of this paper offers the following:

- We offer a method to derive an equivalent permanent magnet (ePM) such that the magnetic field of a multilayer EM can be characterized by a distributed set of multi-poles (DMP) model; the procedure to derive the DMP for a PM can be found in [8]. With all the magnetic fields of the PMs and EMs in a system are modeled as DMP, the magnetic forces on the system can be calculated using the Maxwell stress tensor method or the dipole force model (1).

- The DMP model derived for a cylindrical ML coil has been validated by comparing the computed magnetic fields against exact solutions computed from the original ML coil for a range of aspect ratios. In addition, we compare the magnetic force computed using the dipole force equation (1) against results of the Lorentz force equation and the Maxwell stress tensor method, and validate the comparisons against published experimental data. Unlike the Lorentz force equation and the Maxwell stress tensor method, both of which require computationally tedious volume and surface integrations respectively, the closed-form dipole force equation (replacing integrations with summations) dramatically reduces computation time.

- Along with the CAD design, we illustrate the application of the ePM and dipole force model for simulating the maximum current inputs required for a given design.

II. DMP MODEL OF A MULTILAYER EM

To model a multilayer EM as an equivalent permanent magnet (ePM), the process involves finding an equivalent magnetization **M** in terms of the current density **J** and coil geometry, which specifies the voice coil. Once the ePM is found, a distributed set of magnetic dipoles that characterizes the magnetic field of the EM can be derived using the distributed multi-pole (DMP) modeling procedure [8].

The magnetic flux density created at $\mathbf{R}'(x', y', z')$ due to the current-carrying EM to the field point $\mathbf{R}(x, y\,z)$ is given by the Biot-Savart law [9]:

$$\mathbf{B}_{EM} = \frac{\mu_0}{4\pi} \int_V \frac{\mathbf{J} \times (\mathbf{R}' - \mathbf{R})}{|\mathbf{R}' - \mathbf{R}|^3} dV \tag{2}$$

For a PM, the magnetic flux density can be calculated from the negative gradient of the analytical magnetic potential [9]:

$$\mathbf{B}_{PM} = \frac{\mu_0}{4\pi} \int_V \frac{-(\nabla \bullet \mathbf{M})(\mathbf{R}' - \mathbf{R})}{|\mathbf{R}' - \mathbf{R}|^3} dV + \frac{\mu_0}{4\pi} \int_S \frac{(\mathbf{M} \bullet \mathbf{n})(\mathbf{R}' - \mathbf{R})}{|\mathbf{R}' - \mathbf{R}|^3} dS \tag{3}$$

Unlike (2), the calculation of $\mathbf{B}_{PM}$ does not need the cross product of **J** and **R - R'** vectors. Equations (2) and (3) provide the basis for deriving an ePM for the multilayer EM. The interest here is to seek the field solution outside the physical region of the electromagnet, particularly near its boundary along the magnetization axis. The procedure is best illustrated through an example.

Cylindrical EM

Cylindrical PMs and EMs are commonly used. Some analytical and experimental results are also available for model validation. They are used here for clarity to illustrate the DMP modeling procedure. Figures 2(a) and (b) show the geometry of a cylindrical EM and its corresponding ePM. The current density of the EM is given by (4):

$$\mathbf{J} = J(r)\mathbf{e}_{\theta} \quad \text{where} \begin{cases} J(r) = 0, & 0 \leq r < a_i \\ J(r) = J, & a_i \leq r \leq a_o \end{cases} \tag{4}$$

and a_i and a_o are the inner and outer coil radii.
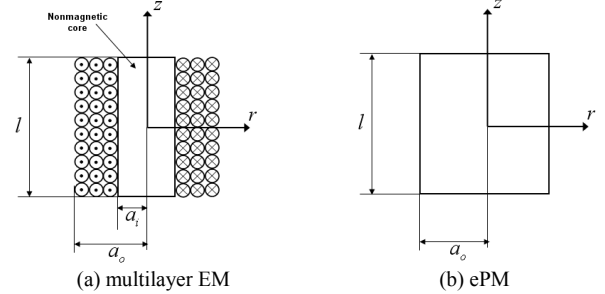

(a) multilayer EM (b) ePM
Fig. 2 Multilayer EM and Equivalent PM

From (2), the z-component of the EM flux density can be calculated, which yield

$$\frac{\mathbf{B}_{EMz}(X',Y',Z')}{\mu_0 J(l/2)} =$$

$$\frac{1}{4\pi} \int_{a_i/a_o}^{1} \int_{-1}^{1} \int_{0}^{2\pi} \frac{R(R - X'\cos\theta - Y'\sin\theta)d\theta dRdZ}{\left[(X' - R\cos\theta)^2 + (Y' - R\sin\theta)^2 + L^2(Z' - Z)^2\right]^{3/2}} \tag{5}$$

where $(X',Y',Z') = (x'/a_o, y'/a_o, 2z'/l)$; and $L = l/(2a_o)$. The effect of the aspect ratios, a_i/a_o and $l/(2a_o)$, on the EM flux density is graphed in Figs. 3(a)-(c), where the z component B_{EMz} at $\varepsilon/l = 0.01$ is normalized to $\mu_0 Jl/2$ and plotted along the radial direction.

As shown in Fig. 3, B_{EMz} is relatively uniform inside the air core, and linearly decreases along the radial direction. The maximum B_{EMz} occurs at $X'=Y'=0$:

$$\frac{B_{EMz}(0,0,l/2+\varepsilon)}{\mu_0 Jl/2} = \ln\left(\frac{a_o + R_{o-}}{a_i + R_{i-}}\right) + \frac{\varepsilon}{l}\ln\left(\frac{(a_o + R_{o-})(a_i + R_{i+})}{(a_i + R_{i-})(a_o + R_{o+})}\right) \tag{6}$$

where ε is any positive number; $R_{o+} = \sqrt{\varepsilon^2 + a_o^2}$; $R_{i+} = \sqrt{\varepsilon^2 + a_i^2}$; $R_{o-} = \sqrt{(l+\varepsilon)^2 + a_o^2}$; and $R_{i-} = \sqrt{(l+\varepsilon)^2 + a_i^2}$.
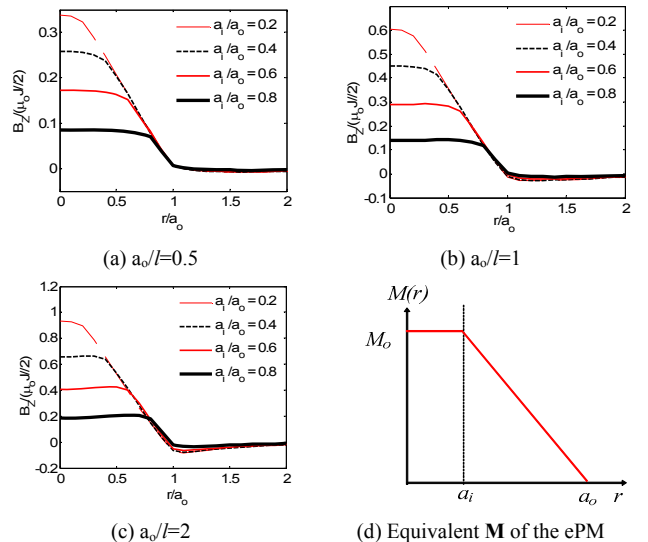

(a) a_o/l=0.5

(b) a_o/l=1

(c) a_o/l=2

(d) Equivalent **M** of the ePM

Fig. 3 Effect of a_i/a_o and $l/(2a_o)$

3336

Equivalent Magnetization of the ePM

For a cylindrical PM, **M** is zero outside the physical boundary where $r \geq a_o$. This, along with the observation in Figs. 3(a)-(c), suggests that the magnetization of the ePM takes the following form:

$$\mathbf{M} = M(r)\mathbf{e_z} \quad \text{where} \begin{cases} M(r) = M_o, & 0 \leq r < a_i \\ M(r) = M_o - J(r - a_i), & a_i \leq r \leq a_o \end{cases} \quad (7)$$

where M_0 is an integral constant to be found by comparing (2) and (3). Since the cylindrical ePM has a maximum along its magnetization, we find M_0 from $B_{PMz} = B_{EMz}$ at $(0, 0, l/2 + \varepsilon)$. Substituting (7) into (3) and noting that $\nabla \bullet \mathbf{M} = 0$, the first term on the right side of (3) disappears and we have (8):

$$\frac{B_{PMz}(0, 0, l/2 + \varepsilon)}{\mu_0 Jl/2} = \ln\left(\frac{a_o + R_{o-}}{a_i + R_{i-}}\right) + \frac{\varepsilon}{l}\ln\left[\frac{(a_o + R_{o-})(a_i + R_{i+})}{(a_i + R_{i-})(a_o + R_{o+})}\right] + \frac{1}{Jl}\left[J(a_o - a_i) - M_0\right]\left(\frac{\varepsilon}{R_{o+}} - \frac{l+\varepsilon}{R_{o-}}\right) \quad (8)$$

M_0 can now be determined by equating (6) and (8), which implies that the last term of (8) must be zero. As the factor involving the independent variable ε is not always zero, $M(r) = J(a_o - a_i)$. Hence, the equivalent magnetization **M** graphically illustrated in Fig. 3(d) is given by (9):

$$\mathbf{M} = M(r)\mathbf{e_z} \quad \text{where} \begin{cases} M(r) = J(a_o - a_i), & 0 \leq r < a_i \\ M(r) = J(a_o - r), & a_i \leq r \leq a_o \end{cases} \quad (9)$$

Once the ePM is found, the EM can be modeled using a distributed set of multipoles (DMP) [8]. For a cylindrical PM, the DMP consists of k circular loops of n equally spaced dipoles parallel to the magnetization vector as shown in Fig. 4. The loops (each with radius $\overline{a}_j$) are uniformly spaced:

$$\overline{a}_j = aj/(k+1) \text{ at } z = \pm\overline{l}/2 \ (0 \leq j \leq k) \quad (10)$$

The flux density at point P(x, y, z) can be computed using (11):

$$\mathbf{B} = \frac{\mu_0}{4\pi}\sum_{i=0}^{k}m_i\sum_{j=1}^{n}\left(\frac{\mathbf{R}_{ij+}}{|\mathbf{R}_{ij+}|^3} - \frac{\mathbf{R}_{ij-}}{|\mathbf{R}_{ij-}|^3}\right) \quad (11)$$

where $\mathbf{R}_{ij+}$ and $\mathbf{R}_{ij-}$ are the vectors from the source and sink of the ith dipole on the jth loop to P respectively.
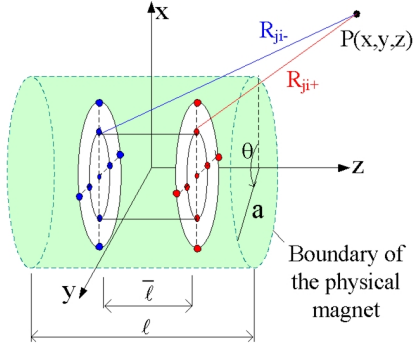

Fig. 4 DMP model of a cylindrical magnet [8]

The force acting on the PM can be computed by summing the individual forces on the magnetic dipoles using (1).

III. MODEL VALIDATION

To validate the DMP derived for a circular EM, we investigate the effect of DMP models on a) the magnetic field distribution, and b) the magnetic force computation. Test setups and computed results for the above case studies are discussed in the following subsections.

A. Validation of magnetic field computation

We compare the DMP$_{EM}$ modeled magnetic field against the exact solution using (3) integrating over the original multilayer EM 3D geometry, and the ESL approximation. Along with the parameters that characterize the ESL and DMP$_{EM}$, Table 1 lists the dimensions of four multilayer (ML) EMs which use 28AWG wire.

TABLE 1: EM COIL* GEOMETRIES AND THEIR ESL AND DMP MODELS

		EM1	EM2	EM3	EM4
ML	a_o (mm)	9.53	9.53	12.7	15.88
	a_i/a_o	0.66	0.5	0.375	0.3
	$l/(2a_o)$	1	1	0.5	0.3
ESL	$J_e d_w$ (A/mm)	31.78	48.0	82.12	120.14
	a_e (mm)	9.08	8.76	10.28	12.0
DMP	$n, k, \overline{l}/l$	12, 6, 0.812	12,6, 0.8142	12, 4, 0.621	16, 6, 0.442
	m_i (µA/m)	0.062, 0.046, 0.104, 0.148, 0.238, 0.367, -0.014	0.081,0.078, 0.133,0.311, 0.343,0.211, 0.0195	0.774, 0.498, 1.347, 1.018, 0.522	1.476, 0.547, 1.618, 1.644, 1.654, 1.325, 0.592

*28AWG Wire with 1A Current

Since the magnetic flux density of the ESL model is singular at the surface ($z=l/2$), we plot in Fig. 5 B_z at $z=l/2+\varepsilon$ where $\varepsilon=0.55$mm for the four EMs to show the effect of aspect ratios (a_i/a_o and $l/2a_o$) on B_z. Typical B_r at $z=l/2+\varepsilon$ and B_z along the z axis are given in Fig. 6, where EM2 is based.

The DMP$_{EM}$ models agree very well with the exact integral of the multilayer EMs. The ESL models closely predict the flux density along the z-axis and for thin coil ($a_i/a_o \approx 1$), but the discrepancies from the exact solutions increase with smaller a_i/a_o (or thicker coils) as shown in Figs. 5 and 6.
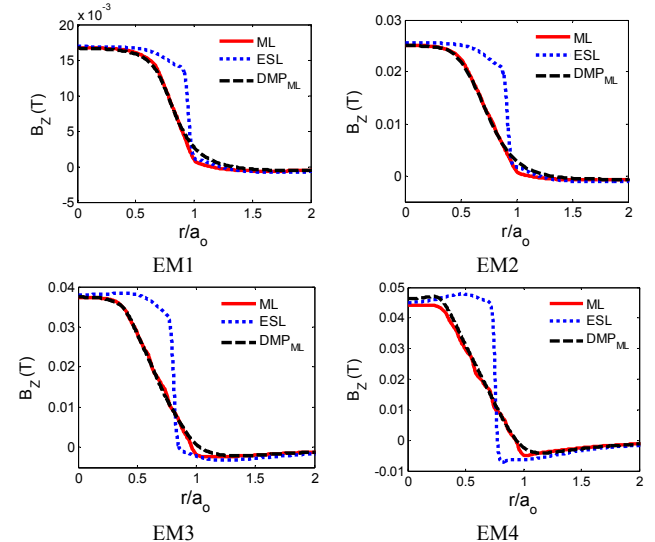

Fig. 5 B_{PMz} in Tesla ($\varepsilon=0.55$mm)

3337

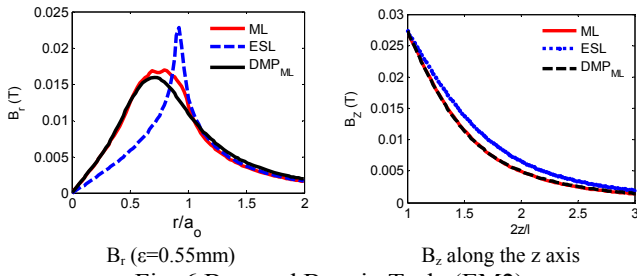B_r (ε=0.55mm)　　　　　B_z along the z axis
Fig. 6 B_{PMr} and B_{PMz} in Tesla (EM2)

B. Validation of magnetic force computation

We compute the magnetic force between a PM and an EM for the test setup shown in Fig. 7 using three different methods, and compare the results against published experimental data [10]. In all three methods, the PMs are all modeled as DMP.

Method I: Maxwell Stress Tensor $\mathbf{T}$ with the multilayer EM.

$$\mathbf{F} = \oint_C \mathbf{T}\,dC \qquad (12)$$

where $\mathbf{T} = \dfrac{1}{\mu_0}\left(\mathbf{B}(\mathbf{B}\bullet\mathbf{n}) - \dfrac{1}{2}B^2\mathbf{n}\right)$; and

C is an arbitrary boundary enclosing the body of interest; and $\mathbf{n}$ is the normal of the boundary interface. Equation (12) requires the total field $\mathbf{B}$ (contributed by both the PM and EM) to compute the force by the surface integration.

Method II: Lorentz force equation with the ESL model replacing the multilayer EM.

$$\mathbf{F} = -\oint \mathbf{B} \times Id\mathbf{n} \quad \text{where } I = \iint J dS \qquad (13)$$

where $\mathbf{n}$ is the unit current direction vector; and S is the cross section of wire. Since the current density vector $\mathbf{J}$ is directly used in the calculation, only the $\mathbf{B}$-field of the PM is needed in the Lorenz force equation, which calculates the magnetic force exerted on current-carry EM.

Method III: Dipole force equation with the DMP of EM

With the EM and PM modeled as respective DMPs, the force acting on each of the dipoles under the influence of the current-carry EM can be calculated from (1) where $\mathbf{H} = \mathbf{B}/\mu_0$; and $\mathbf{B}$ is given by (11). The net force acting on the PM is simply the summation of the individual forces on the dipoles that characterize the PM:

$$\mathbf{F} = \frac{\mu_0}{4\pi}\sum_{i=1}^{n_r} m_{r_i}\sum_{j=1}^{n_s} m_{s_j}\left(\mathbf{R}_{s_{j+}r_{i+}} - \mathbf{R}_{s_{j+}r_{i-}} + \mathbf{R}_{s_{j-}r_{i-}} - \mathbf{R}_{s_{j-}r_{i+}}\right) \qquad (14)$$

In (14), $\mathbf{R}_{s_\pm r_\pm} = (\mathbf{R}_{s\pm} - \mathbf{R}_{r\pm})/|\mathbf{R}_{s\pm} - \mathbf{R}_{r\pm}|^3$; and n_r and n_s are the number of dipoles of the PM and EM respectively.

Size	Large	Small
d_1 (mm)	3.048	1.524
d_2 (mm)	3.962	3.175
d_3 (mm)	2.998	1.6
L (mm)	1.6	0.813
Coil res. (Ω)	57	32
Wire length (m)	3	1.68

Samarium-Cobalt magnet; $\mu_0 M_0$=1.02 T
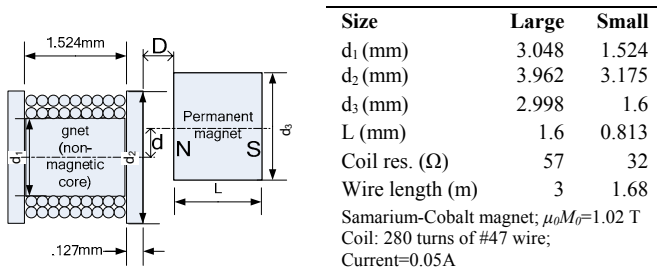Coil: 280 turns of #47 wire;
Current=0.05A

Fig. 7 Experimental setup and parameters

Table 2 summarizes the parameters used in this simulation, for the two setups shown in Fig. 7. Figure 8 compares the computed forces against published experimental data; and Table 3 compares the error for each case and the time required to compute 26 data points for the case in Fig. 8(a) using a computer with Quad Core 2.66GHz CPU and 8G RAM. And the error is defined as

$$Error = \sum\left|F - F_{exp}\right| / \sum\left|F_{exp}\right|$$

As shown in Fig. 8, the results computed using the dipole force equation closely agrees with the experimental data.

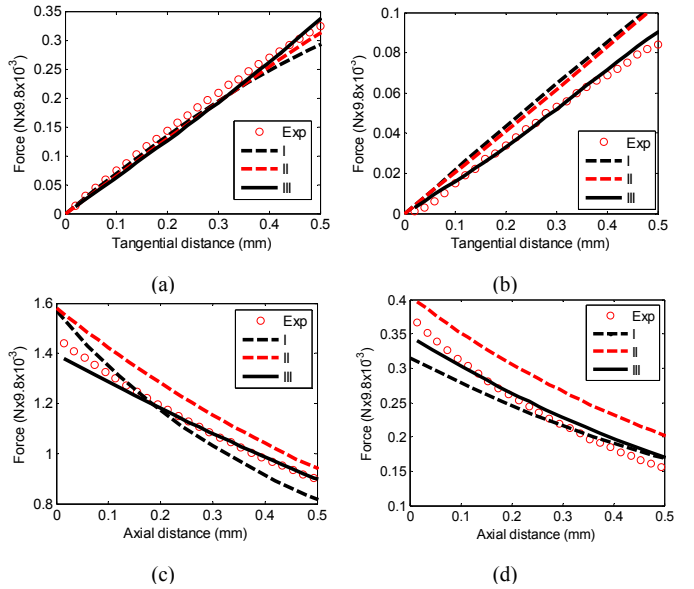
(a)　　　　　　　　(b)

(c)　　　　　　　　(d)
Fig. 8 Computed forces and experimental data

For all cases, the Maxwell stress tensor and the dipole force equation (or Methods I and III respectively) very closely agree with published experimental data while the ESL model (that reduces the volume integral of the multi-layer EM to surface integral of a single-layer coil) overestimates the computed forces as expected. Unlike the Lorentz force equation (with the ESL approximation) and the Maxwell stress tensor method requiring computationally tedious surface integrations, the closed-form dipole force equation (replacing integrations with summations) dramatically reduces the computation time.

TABLE 2: SIMULATION PARAMETERS

	Parameters	Large	Small
PM DMP$_{PM}$	$\mathbf{n}, \mathbf{k}, \bar{l}/l$	6, 2, 0.314	6, 2, 0.3122
	m_i (μA/m)	1.65, 0.02, 3.8	0.43, 0.02, 1.07
EM (ESL)	$J_c d_w$ (μA/mm)	22.75	38.98
	a_e (mm)	1.8168	1.456
EM (DMP$_{EM}$)	n, k, $\bar{l}/l$	12, 8, 0.7661	8, 3, 0.7441
	m_i (nA/m)	0.236, 0.177, 0.366, 0.567, 0.751, 0.914, 1.032, 1.28, 0.312	1.354, 1.758, 3.32, 1.661

TABLE 3: COMPARISON OF COMPUTATION TIME AND ERROR

Method		I	II	III
Error (%)	Fig. 8(a)	6.02	7.55	6.29
	Fig. 8(b)	21.1	26.4	3.89
	Fig. 8(c)	3.2	7.1	2.2
	Fig. 8(d)	10.3	16.4	12.4
Computation Time (sec)		106.03	21.53	0.0625

3338

IV. Illustrative Application

As illustrated in the above example, the dipole force equation with EMs and PMs modeled as DMP is an efficient way to compute the magnetic force in 3D space for design and control of an electromagnetic system, especially for wrist-like spherical motors [8] where a large number of stator EM coils and PMs are involved.

Figure 9 shows the CAD model of a spherical motor, where the PMs and EMs are equally spaced on layers of circular planes with their radial magnetization axes passing through the motor center, where the EMs are air-cored; and the entire structure (except for the PMs) is non-magnetic. The PMs and EMs are grouped in pairs such that they are electromechanically symmetric. The spherical motor design has 3 layers of 8 stator EMs, and 2 layers of 12 rotor PMs. The magnetization axes of these PMs or EMs, can be characterized mathematically by a vector. The magnetization axes of the m_r PM pole-pairs are given in rotor coordinates (x,y,z) by (15):

$$\mathbf{r}_i = (-1)^{i-1}\left[\cos\theta_{ri}\cos\phi_{ri} \quad \cos\theta_r\sin\phi_{ri} \quad \sin\theta_{ri}\right]^{\mathrm{T}} \quad (15)$$

Similarly, the m_s EM pole-pairs in the stator frame (XYZ) are

$$\mathbf{s}_j = \left[\cos\theta_{sj}\cos\phi_{sj} \quad \cos\theta_{sj}\sin\phi_{sj} \quad \sin\theta_{sj}\right]^{\mathrm{T}} \quad (16)$$

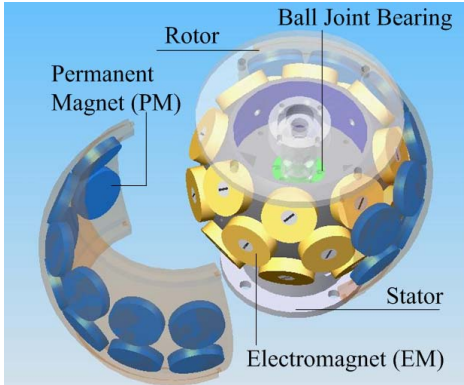In (15) and (16), (θ_r,ϕ_s) and (θ_s,ϕ_r) are given in Table 4.

Fig. 9 CAD model of the spherical motor

Because of the symmetry, the EM current inputs are designed such that

$I_1=I_{13}=u_1$, $I_2=I_{14}=u_2$, $I_3=I_{15}=u_3$, $I_4=I_{16}=u_4$, $I_5=I_9=u_5$, $I_6=I_{10}=u_6$,

$I_7=I_{11}=u_7$, $I_8=I_{12}=u_8$, $I_{18}=I_{19}=-I_{22}=-I_{23}=u_9$,

$I_{17}=-I_{20}=-I_{21}=I_{24}=u_{10}$.

The design has the operating range

$$0 \leq (\psi,\phi) \leq 360° \text{ and } -22.5 \leq \theta \leq 22.5°$$

where (ψ,θ,ϕ) are the ZYZ Euler angles of the rotor.

TABLE 4: DESIGN PARAMETERS

	Rotor			Stator	
i	θ_r(deg)	ϕ_r(deg)	j	θ_s(deg)	ϕ_s(deg)
1-12	-15	30(i-1)	1-8	26	45(j-1)
13-24	15	30(i-13)	9-16	-26	45(j-9)
			17-24	0	45(j-17)+22.5

A. Torque-Current Relationship of a Spherical Motor

The torque model of the PM-based spherical motor with linear magnetic properties has the following form:

$$\mathbf{T} = \left[T_X \ T_Y \ T_Z\right]^{\mathrm{T}} = [\mathbf{K}]\mathbf{u} \quad (17)$$

where

$$\mathbf{K}\left(\in \mathbb{R}^{3\times m_s}\right) = \left[K_1 \ \cdots \ K_p \ \cdots \ K_{m_s}\right] \quad (18)$$

and

$$\mathbf{u} = \left[I_1 \ \cdots \ I_p \ \cdots \ I_{m_s}\right]^{\mathrm{T}} \quad (19)$$

In (17), I_p is the current input in the pth EM; m_s is the total number of EMs; and $K_p \in \mathbb{R}^{3\times 1}$. The torque characteristic vector K_p (contributed by the pth EM to the whole rotor) at each rotor orientation (ψ,θ,ϕ) can be derived using dipole method. Given that each of the EMs (or PMs) is characterized by n_p (or n_r) number of dipoles, we have

$$K_p = \frac{\mu_0}{4\pi}\sum_{i=1}^{n_r}m_{r_i}\sum_{j=1}^{n_p}m_{s_j}\left[\left(\mathbf{R}_{s_{j+}r_{i+}} - \mathbf{R}_{s_{j-}r_{i+}}\right)\times\mathbf{R}_{r_{i+}} - \left(\mathbf{R}_{s_{j+}r_{i-}} - \mathbf{R}_{s_{j-}r_{i-}}\right)\times\mathbf{R}_{r_{i-}}\right] \quad (20)$$

Since the SWM has more current inputs than its mechanical degrees of freedom, the actual current input vector $\mathbf{u}$ for a given torque is found by minimizing the input energy consumption subject to the desired torque constraint. Provided that the input currents are kept within limits, the optimal $\mathbf{u}$ can be solved using Lagrange multipliers. The optimal solution [4] can be written in closed form:

$$\mathbf{u} = [\mathbf{K}]^{\mathrm{T}}\left([\mathbf{K}][\mathbf{K}]^{\mathrm{T}}\right)^{-1}\mathbf{T} \quad (21)$$

B. Current needed for a Specified Torque

The end-effecter is mounted on the spherical rotor, and is designed such that the center of gravity coincides with the rotation center as shown in Fig. 10. The external torque is

$$T_{ext} = r \times m_{load}g \quad (22)$$

Statically, the torque acting on the rotor is equal to the external torque at any orientation, and thus the current input in each EM at (ψ,θ,ϕ) can be determined from (17). Table 5 summarizes the parameters used in this simulation. The maximum current of each EM in a full circle ($0 \leq \phi \leq 360°$) was recorded and shown in Fig. 11. Specifically, the input profiles were plotted in the range of $0 \leq \psi \leq 90°$ and $-22.5 \leq \theta \leq 22.5°$ due to symmetry.

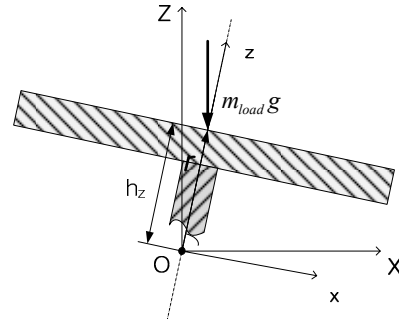Fig. 10 Table model and loading torque

TABLE 5: SIMULATION PARAMETERS

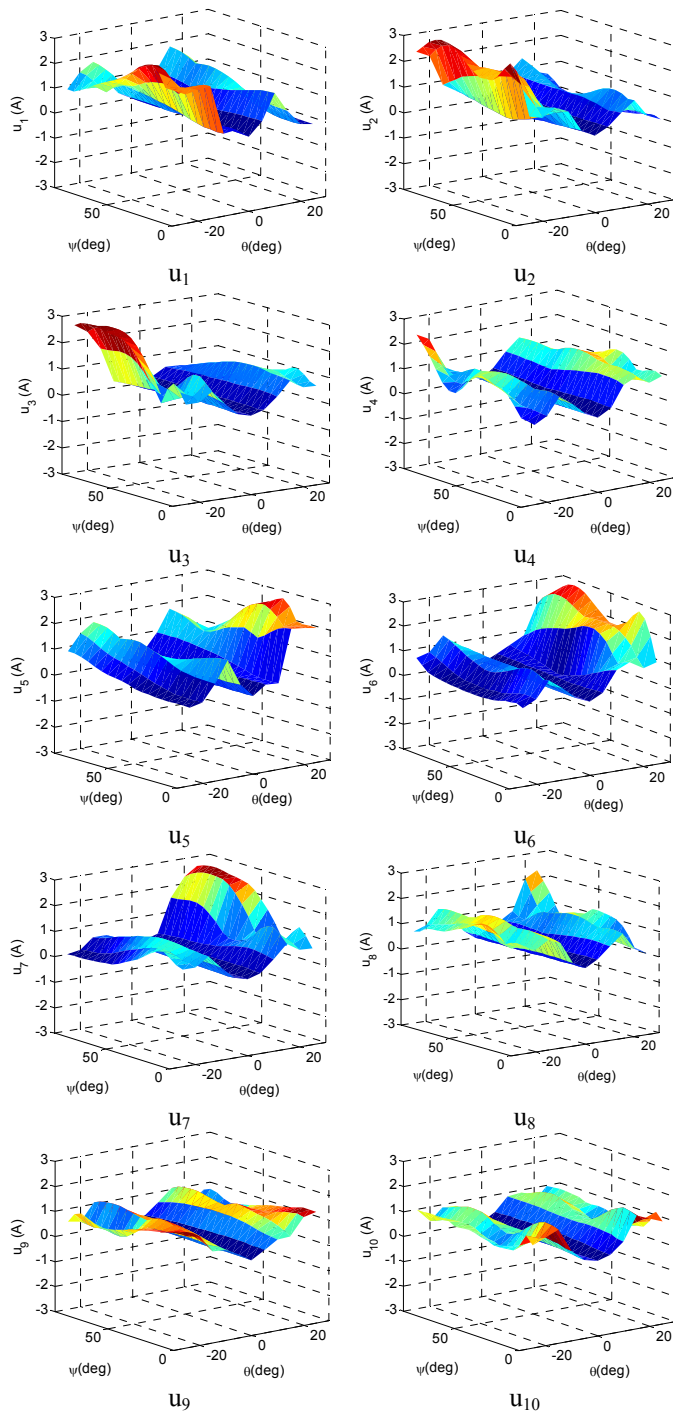| Load	m_{load}	8kg
Rotor	h_z	64.8mm
	mass	2.03kg
	Offset of mass center	0
	Moment of Inertia (kg-m²)	I_{zz}=7.97e-3, I_{xx}=I_{yy}=5.89e-3

3339

Fig. 11 Current inputs in stator

V. CONCLUSIONS

We have presented a new method (that models the multilayer EM as an equivalent PM) for computing the magnetic forces and torques of a electromagnetic actuator system consisting of EMs and PMs. The method has been validated by comparing results against exact field solutions and published experimental force data. Along with the prototype CAD design, we simulate the maximum current inputs required of the spherical motor (150mm×150×150mm) for a given design specifications. The simulation suggests that the maximum current per coil required is less than 3A for the specified load (and rotor weight) of 10kg.

REFERENCES

[1] Lee, K.-M. and C. Kwan, "design concept development of a spherical stepper for robotic applications", *IEEE Trans. On Robotics and Automation*, Feb. 1991. 7(1), pp175-181.
[2] Wang, J., G. Jewell, and D. Howe, "Design and control of a novel spherical permanent magnet actuator with three degrees of freedom", *IEEE/ASME Trans. On Mechatronics*, Dec. 2003. 8(4), pp.457.
[3] Liang, Y., I. M. Chen, G. Yang, L. Wei, and K.-M. Lee, "Analytical and experimental Investigation on the Magnetic Field and torque of a Permanent Magnet Spherical Actuator," *IEEE/ASME Trans. On Mechatronics*, Aug. 2006. 11(4), pp.409-419.
[4] Lee, K.-M., R. A. Sosseh and Z. Wei, "Effects of the Torque Model on the Control of a VR Spherical Motor," *IFAC Journal of Control Engineering Practice,* Nov. 2004. 12(11), pp 1437-1449.
[5] Li, Qiang and K.-M. Lee, "An adaptive meshless computation method for design of electromechanical actuators," *IEEE Trans. On Magnetics*, Aug. 2006. 42(8), pp.1996-2002.
[6] Lee, K.-M. and H. Son, "Distributed Multi-Pole Model for Design of Permanent-Magnet-based Actuators," *IEEE Trans. Magnetics*, Vol. 43, No. 10, pages 3904-3913, October 2007.
[7] K.-M. Lee, H. Son, and J. Joni, "Concept Development and Design of a Spherical Wheel Motor (SWM)," Proc. of the *IEEE ICRA*, April 18-22, Barcelona, Spain, 2005, pp. 3652- 3657.
[8] Son, H. and K.-M. Lee, "Distributed Multi-Pole Models for Design and Control of PM Actuators and Sensors," *IEEE/ASME Trans. Mechatronics*, Vol. 13, No. 2, pages 228-238, April 2008.
[9] Jackson, J.D. "Classical Electrodynamics", New York: Wiley 1999.
[10] Bastos, N.I.J.P.A. "Forces in permanent magnets team workshop problems 23," http://www.compumag.co.uk/team.html.